Title: Boundary conditions for synaptic homeodynamics during the sleep-wake cycle

Authors: Fukuaki L. Kinoshita[1,2], Rikuhiro G. Yamada[2,3], Koji L. Ode[4], Hiroki R. Ueda[2,3,4*]

Affiliations:

[1]Department of Neurology, Graduate School of Medicine, Osaka University, 565-0871 Osaka, Japan

[2]Laboratory for Synthetic Biology, RIKEN Center for Biosystems Dynamics Research, 565-0871 Osaka, Japan

[3]Department of Systems Biology, Institute of Life Science, Kurume University, 830-0011, Fukuoka, Japan

[4]Department of Systems Pharmacology, Graduate School of Medicine, The University of Tokyo, 113-0033 Tokyo, Japan

*Corresponding author. Email: Email: uedah-tky@umin.ac.jp

Abstract

Understanding synaptic dynamics during the sleep-wake cycle is crucial yet controversial. While some studies report synaptic depression during non-rapid eye movement (NREM) sleep, others observe synaptic potentiation. To find boundary conditions between these contradictory observations, we focused on learning rules and firing patterns that contribute to the synaptic dynamics. Using computational models, we found that under Hebbian and spike-timing dependent plasticity (STDP), wake-like firing patterns decrease synaptic weights, while sleep-like patterns strengthen synaptic weights. Conversely, under Anti-Hebbian and Anti-STDP, synaptic depression during NREM sleep was observed, aligning with the conventional synaptic homeostasis hypothesis. Moreover, synaptic changes depended on firing rate differences between NREM sleep and wakefulness. We provide a unified framework that could explain synaptic homeodynamics under the sleep-wake cycle.

Main Text

Introduction

During wakefulness, organisms perceive external worlds through the five senses to learn and take appropriate actions. During sleep, organisms disconnect from the environment to reorganize memory and recover from fatigue. Recent studies have revealed that cortical neurons are responsible for these brain functions underlying learning and memory formation (*1*) and that the dynamics of the cortical synaptic weights are associated with the sleep-wake cycle (*2*, *3*). A hypothesis known as the synaptic homeostasis hypothesis (SHY) proposed that wakefulness potentiates synapses through learning with the costs of higher energy demand while the sleep state depresses less important synapses to restore synaptic homeostasis (*2*). However, the dynamics of synaptic weights in the sleep-wake cycle, especially during sleep, remain controversial. Several studies have demonstrated that NREM sleep potentiates synapses, contributing to memory consolidation (*4*, *5*). Furthermore, SHY suggests that synapses strengthened during wakefulness are less susceptible to synaptic depression during NREM sleep (*2*). In contrast, other studies propose the normalization of neuronal activities, where fast-firing neurons and slow-firing neurons during wakefulness are weakened and strengthened, respectively, during NREM sleep (*6*). We sought to find the boundary conditions that reconcile these discrepancies and to comprehensively understand the sleep-wake synaptic dynamics.

The heterogeneity of brain states can confound in vivo studies because the slow-wave oscillation (SWO), that is a characteristic firing pattern of NREM sleep, also occurs in wakefulness and sleep states include REM sleep, which has wake-like firing patterns (*7*, *8*). To address this issue, we developed computational models to investigate the direct relationships between synaptic weights and neuronal firing patterns characteristic of each brain state. To account for the diversity of neurons, we prepared various sleep- and wake-like firing patterns based on in vivo experiments. Additionally, we devised a unified function that recapitulates typical synaptic learning rules in the

cortex for updating the synaptic weights (*9*). These settings allowed us to simulate the dynamics of synaptic weights under specific types of spike trains, such as burst firing, based on synaptic learning rules (*10*). The synaptic learning rules we studied include the Hebbian rule, STDP, and their reverse types (Anti-Hebbian and Anti-STDP). According to the Hebbian rule, a synaptic connection between two neurons strengthens when pre- and post-synaptic neurons fire simultaneously (*11*). A temporally asymmetric form of Hebbian rule is STDP. The classical STDP describes that synaptic potentiation occurs when pre-synaptic spikes precede post-synaptic spikes within a certain temporal window, while synaptic depression occurs in post-synaptic spikes precede pre-synaptic spikes (*12*). Reverse types of them (Anti-Hebbian and Anti-STDP) are also observed in the mammalian cortex (*13*) and play important roles in information processing (*14*).

Our simulations revealed that synaptic weights become higher in sleep-like synchronized states than in wake-like desynchronized states under Hebbian and classical STDP, assuming the same mean firing rates for both sleep- and wake-like firing patterns. We refer to these dynamics as Wake Inhibition and Sleep Excitation (WISE). In contrast, synaptic depressions during sleep-like firing patterns, which represents SHY, were observed under Anti-Hebbian and Anti-STDP. Moreover, our results suggested that the synaptic dynamics also depend on mean firing rates, providing a unified framework for the synaptic homeodynamics of neural networks during the sleep-wake cycle.

Results

WISE under Hebbian and STDP, SHY under Anti-Hebbian and Anti-STDP

To investigate synaptic dynamics in NREM sleep and wakefulness with synaptic learning rules, we used a Ca^{2+}-based plasticity model. Graupner et al. proposed that the Ca^{2+}-based plasticity model with two thresholds for post-synaptic Ca^{2+} can describe the various types of synaptic learning rules

(*15*). Based on Graupner's model, we developed a modified Ca^{2+}-based plasticity model to represent four different types of learning rules (Hebbian, STDP, Anti-Hebbian, and Anti-STDP) by setting eight parameters (θ_p: potentiation threshold, θ_d: depression threshold, γ_p: potentiation amplitude, γ_d: depression amplitude, τ_{pre}: time constant for Ca^{2+} from NMDAR (N-methyl-D-aspartate receptor), τ_{post}: time constant for Ca^{2+} from VGCC (Voltage-gated Ca^{2+} channel), σ: amplitude for noise, and τ_s: time constant for synaptic change) (**Fig. 1A** and **supplementary text I A**). We confirmed that our model could predict the experimentally observed changes of post-synaptic Ca^{2+} and synaptic strength under stimulations with different time lags (**Fig. 1, B** and **C**). We randomly generated more than 1 million parameter sets and selected 1,000 parameter sets that well represent either one of four learning rules (**Fig. 1, D** and **E**, and **supplementary text I B**). Each learning rule has a clear cluster in the distribution of thresholds and amplitudes (**Fig. 1F**). The distributions of other parameters and those in other fitting conditions are shown in fig. S1. To evaluate the change of synaptic weights during sleep-like and wake-like firing patterns, we assumed one post-neuron connected with ten pre-neuronal synapses and the same mean firing rates both in sleep-like and wake-like patterns (**Fig. 1G** and **supplementary text I D**). Firing patterns were derived from previous in vivo recordings (*6*, *16*) (fig. S18 and **supplementary text I E**) and synaptic weights were defined as being linearly related to synaptic efficacy (*ρ)* (*Eq.* 1 in **supplementary text I A**) (*15*). With the setting, the mean synaptic efficacy became higher in sleep-like states than in wake-like states under Hebbian and STDP, representing WISE (**Fig. 1H**). The opposite results were observed in Anti-Hebbian and Anti-STDP, representing SHY. Thus, WISE and SHY are observed under the specific types of learning rules, with both states exhibiting equal mean firing rates.

Robustness of WISE and SHY

Next, we investigated the robustness of the WISE and SHY in different settings. We first simply extended the previous model with one post-neuron connected by ten pre-neuronal synapses to have 96 pre-neuronal synapses. This extended model still exhibited WISE under Hebbian and STDP, while it showed SHY under Anti-Hebbian and Anti-STDP (**Fig. 2A**). Next, we tested a randomly connected model and modified parameters of time constants and amplitudes of learning rules to see if WISE and SHY depend on the properties of learning rules. Even in those settings, we found that these trends still held (**Fig. 2, B** and **C**, and **fig. S3**). In Fig. 2, D and E, we generated various sleep-like firing patterns by changing parameters such as the log10(*mean inter-spike interval*) (ISIM), log10(*mean Up-state duration*) (UPM), and log10(*mean Down-state duration*) (DOWNM). We tested ranges of parameters for each targeted mean firing rate by changing either DOWNM (**Fig. 2D**) or ISIM (**Fig. 2E**). We found that the mean synaptic efficacy was higher in sleep-like states with most of the parameters in the tested range. Notably, this trend was more apparent at lower firing rates. These results validated that WISE and SHY were robust under various biologically feasible conditions.

WISE and SHY in Hodgkin-Huxley-based network models

We then tested whether WISE and SHY hold in a more realistic setting where the synaptic efficacy can change the firing pattern. To recapitulate the variable firing pattern, we introduced the Hodgikin-Huxley model to network models based on our previous study (*17*), with a ratio of excitatory and inhibitory neurons of 4:1 (**Fig. 3A** and **supplementary text II**). In this study, we considered molecules responsible for generating SWO in three subcellular compartments (post-synaptic, intracellular (cell body), and pre-synaptic compartments) (*17*, *18*). We assumed that NMDAR and VGCC function in post-synapses and cell bodies, respectively, for generating SWO (*17*). In addition, because pre-synaptic transmission is crucial for generating SWO in the cortex

(*18*), we modeled AMPAR, NMDAR, and GABAR to receive the neural transmission. Parameter searches for SWO and bifurcation analysis for a single neuron were based on previous articles (*17*). First, we randomly generated parameter sets from a large parameter space within the biophysically feasible range and searched for parameter sets that yield firing patterns of SWO. Then, we searched for parameter sets that bifurcate from wake-like to sleep-like patterns as a network (**Fig. 3B** and **supplementary text II B**). Clear desynchronization and synchronization, evaluated by a sleep score (**supplementary text IV**), were observed with parameter sets for each subcellular component (**Fig. 3, C and D**, and **fig. S4**). We then selected the parameter sets that showed almost the same mean firing rates in sleep-like and wake-like states and evaluated synaptic efficacy in the sleep-like and wake-like states (**fig. S6** and **S7**). WISE was observed under STDP (**Fig. 3E**), while SHY was observed under Anti-STDP (**Fig. 3F**). Similar trends were observed under Hebbian and Anti-Hebbian and in network models with different connections (**fig. S9** and **S10**). These results validated WISE and SHY in a realistic network model.

WISE under Hebbian and STDP and SHY under Anti-Hebbian and Anti-STDP is compatible with models including sleep-wake dynamics

Next, we incorporated the spontaneous sleep-wake cycle into our network models. Previous phosphoproteomic studies suggested that phosphorylation of several synaptic proteins is associated with sleep needs (*19*, *20*). The sleep needs increase during wakefulness and decreases with the onset of sleep. This homeostatic oscillation of sleep needs is referred to as Process S (*21*). In the present model, we assumed that calcium/calmodulin-dependent protein kinase II (CaMKII) is responsible for the homeostatic oscillation (*22*). To evaluate the synaptic efficacy across a series of sleep-wake cycles, we assumed that CaMKII changes its states in a use-dependent manner during wakefulness and induces SWO by interacting with channels or

162 receptors that regulate neuronal membrane potentials or enzymes that regulate neurotransmitters
163 (*8*, *22*). This assumption aligns with observations that CaMKII has multiple phosphorylation states
164 and changes its function accordingly (*23*). We integrated the use-dependent change of CaMKII's
165 function for activating channels such as NMDAR into the sleep-wake dynamics model (*Eq*. 57-62
166 in **supplementary text III**). The initial state of CaMKII, such as pT286/287 CaMKII, has self-
167 activating ability and Ca^{2+}-dependent activation (*24*). This initial state activates the second state of
168 CaMKII, such as pT305/306 CaMKII, or phosphatases, such as calcineurin, which can be regulated
169 during sleep (*25*). We assumed that the second state directly interacts with molecules that induce
170 SWO from the result of optimizing correlation to Process S for network models (**fig. S11A**).

171 In the simulation of a representative model, we observed that pT286/287 CaMKII, represented as
172 ***r*** in Fig. 4A, gradually increased due to Ca^{2+} influx and autoactivation during wakefulness, which
173 was followed by an increase in pT305/306 CaMKII, represented as ***a*** in Fig. 4A. The increased ***a***
174 then activated NMDAR and induced SWO (**Fig. 4, C** and **D**). The mean synaptic efficacy was
175 higher during sleep-like periods than during wake-like periods under STDP (**Fig. 4, E** and **G**). The
176 opposite results were observed under Anti-STDP **(Fig. 4, F** and **H**). Statistical significances were
177 observed in the analysis with multiple parameter sets (**fig. S11, B** and **C**). The results of model
178 with other bifurcation mechanisms or systems also showed the same trends (**fig. S12** to **S14**).
179 These results confirmed that WISE under STDP and SHY under Anti-STDP are compatible with
180 network models that have sleep-wake dynamics.

181

182 **Synaptic changes depend on firing rates assuming higher firing rates during wake-like**
183 **states**

184 In the previous sections, we compared synaptic efficacies in sleep-like and wake-like states by
185 assuming the same mean firing rates in both states. While this assumption is feasible in brain

regions such as the visual cortex, where firing rates are almost constant between states (*26*), regions such as the somatosensory cortex showed higher firing rates during wakefulness (*27*). To evaluate the synaptic dynamics in the higher firing rates during wake-like states, we assumed that mean firing rates in Up states of sleep-like patterns are equal to those in wake-like patterns and found that WISE was observed at lower mean firing rates while SHY was observed at higher mean firing rates under Hebbian and STDP (**Fig. 5A**). Thus, synaptic efficacies change to different directions depending on mean firing rates assuming higher firing rates during wake-like states.

Discussion

In this study, we investigated how synaptic dynamics interact with firing patterns and learning rules. Under Hebbian and STDP, wake-like firing patterns weaken synapses, while sleep-like firing patterns strengthe synapses. We referred to this tendency as WISE. In contrast, under Anti-Hebbian and Anti-STDP, wake-like and sleep-like patterns tend to strengthen and weaken synaptic efficacies, respectively, which aligns with SHY. When we set the firing rate of the Up state of sleep-like phasic firing patterns equal to the firing rate of wake-like tonic firing patterns, the resulting higher firing rate of wake-like firing pattern tends to strengthen synapses. This indicates that firing rate is the dominant factor in determining the direction of synaptic changes. These findings delineate the boundary conditions of synaptic dynamics during the sleep-wake cycle. We also demonstrated that these boundary conditions are stable under various conditions by using two types of models with numerous parameters derived from biological knowledge.

Boundary conditions in synaptic homeodynamics

From the perspective of homeostasis, SHY proposes that wakefulness strengthens synapses to learn about the environment, while NREM sleep weakens less important synapses to reduce

energy consumption (*2*). Although studies, including anatomical and electrophysiological research, support SHY (*19*, *28*, *29*), several studies have reported contradictory results (*4–6*, *30*).

Our study indicated that the direction of synaptic changes during sleep-like firing patterns depends on synaptic learning rules and firing rates of local networks. Assuming the same mean firing rates in sleep-like and wake-like patterns, SHY is observed under Anti-Hebbian and Anti-STDP (**Fig. 1** to **4**). Additionally, we observed that higher mean firing rates results in smaller differences in synaptic changes between sleep-like and wake-like states (**Fig. 1H** and **2,** and **fig. S9**). This finding suggests that neurons with higher firing rates during wakefulness are less susceptible to synaptic depression during sleep, consistent with SHY (*2*). In contrast, we observed WISE under Hebbian and STDP (**Fig. 1** to **4**). This observation indicated that the maximum firing rates during sleep, particularly in the Up state of SWO, are higher when the mean firing rates are equal in both sleep and wakefulness. The high maximum firing rates in sleep enhance synaptic learning rules, that is, Hebbian and STDP strengthen synaptic weights while Anti-Hebbian and Anti-STDP weaken synaptic weights. In vivo experiments also reported that the higher firing rates or shorter inter-spike interval (ISI) in the Up state of SWO (*6*, *7*, *16*) (**fig. S18**). Higher maximum firing rates lead to greater Ca^{2+} influx and larger changes in synaptic weights during SWO. Additionally, synchronization and hyperpolarized Down states that promote Ca^{2+} influx in the subsequent Up state (*31*) likely contribute to elevated post-synaptic Ca^{2+} during SWO.

We propose that synaptic changes depend on the differences in firing rates between NREM sleep and wakefulness. SHY may occur under STDP when mean firing rates during wakefulness are higher than during NREM sleep (**Fig. 5A**). A simulation showed that synaptic efficacies of neurons which are stimulated during wake-like states change according to SHY (**fig. S15**). Similarly, previous studies have demonstrated that exposure to novel stimuli or enforced wakefulness, conditions expected to increase sleep pressure, result in synaptic downscaling during sleep (*32*, *33*). Conversely, quiet conditions, anticipated to yield lower sleep pressure during

wakefulness, have strengthened synapses during sleep (*32*). These observations align with our proposal because exposure to novel environments or higher activity increases firing rates during wakefulness, leading to SHY. In contrast, the quiet wake causes only limited differences in firing rate between NREM sleep and wakefulness, leading to WISE (**Fig. 5A**). These different responses to the neuronal activities during wakefulness support the idea that NREM sleep normalizes the neuronal activities that are skewed during the wakefulness, as presented by Watson et al (*6*).

Noteworthy, WISE predicts lower post-synaptic Ca^{2+} concentration during wake-like desynchronized firing under Hebbian and STDP. This prediction aligns with the observation that calcineurin, an LTD-related molecule likely to be activated by lower Ca^{2+} concentration during wakefulness, plays a role in excitatory post-neuronal synapses for generating SWO in the following NREM sleep (*34–36*). Another prediction of WISE is synaptic connectivity homeostasis. When synaptic transmission is inhibited, the resulting SWO may strengthen synapses through WISE, compensating for the inhibited transmission. The connectivity homeostasis is also anticipated in the synaptic dynamics during hibernation. Decreases in firing rates and synaptic connections due to low temperatures during hibernation are associated with increases in SWO during NREM sleep and restoration of synaptic connections after hibernation (*37*, *38*), that is contrary to SHY. Since the lower the firing rates, the greater the synaptic potentiation during sleep in our results (**Fig. 1H** and **fig. S9**), WISE may explain synaptic dynamics during the hibernation. Likewise, in depressive disorder, which is characterized by reduced waking activity and dysfunction of AMPAR in frontal cortex (*42*), synaptic increase during NREM sleep may occur.

In conclusion, our study provides a unified framework for the synaptic dynamics during the sleep-wake cycle (**Fig. 5B**). It suggests that SHY, WISE, and the normalization during NREM sleep coexist but occur depending on synaptic learning rules and neuronal activities of networks. Although further studies are needed to investigate relationships between synaptic learning rules, neuronal activities, and synaptic weights, the framework we presented here lays a foundation for

future research.

Synaptic dynamics and brain functions

Our study provides several implications regarding the relationship between synaptic dynamics and brain functions during the sleep-wake cycle. WISE supports the notion that synaptic potentiation in NREM sleep contribute to memory consolidation (*4*, *30*), which can be promoted by STDP (*40*). On the other hand, we revealed that wake-like desynchronized states can lead to synaptic depression under Hebbian and STDP, especially at lower firing rates (**Fig. 1** to **4**). One implication of this inhibition during wakefulness is the enhancement of the signal to noise ratio (SNR) (*41*). Stimulated neurons likely fire at higher rates, and their synaptic efficacies become larger than those of other neurons in the background desynchronized states.

We also found that the variability of synaptic efficacy is higher during wakefulness than in NREM sleep under Hebbian and STDP (**Fig. 4G** and **fig. S12** to **S14,** and **S16**). Several studies suggest that the variability of synaptic efficacies leads to the variability of network activity and reflects probabilistic inference for external worlds and decision-making (*42*, *43*). In this context, our results suggest that awake states, with higher variability of synapses, are advantageous for exploration and behavioral selection.

References and Notes

1. K. H. Jawabri, S. Sharma, *Physiology, Cerebral Cortex Functions* (StatPearls Publishing, 2023).
2. G. Tononi, C. Cirelli, Sleep and the Price of Plasticity: From Synaptic and Cellular Homeostasis to Memory Consolidation and Integration. *Neuron* **81**, 12–34 (2014).
3. J. Seibt, M. G. Frank, Primed to Sleep: The Dynamics of Synaptic Plasticity Across Brain

States. *Front. Syst. Neurosci.* **13**, 2 (2019).

4. S. Chauvette, J. Seigneur, I. Timofeev, Sleep oscillations in the thalamocortical system induce long-term neuronal plasticity. *Neuron* **75**, 1105–1113 (2012).

5. I. Timofeev, S. Chauvette, Sleep slow oscillation and plasticity. *Curr. Opin. Neurobiol.* **44**, 116–126 (2017).

6. B. O. Watson, D. Levenstein, J. P. Greene, J. N. Gelinas, G. Buzsáki, Network Homeostasis and State Dynamics of Neocortical Sleep. *Neuron* **90**, 839–852 (2016).

7. M. Steriade, I. Timofeev, F. Grenier, Natural waking and sleep states: a view from inside neocortical neurons. *J. Neurophysiol.* **85**, 1969–1985 (2001).

8. V. V. Vyazovskiy, U. Olcese, E. C. Hanlon, Y. Nir, C. Cirelli, G. Tononi, Local sleep in awake rats. *Nature* **472**, 443–447 (2011).

9. D. E. Feldman, The spike-timing dependence of plasticity. *Neuron* **75**, 556–571 (2012).

10. P. J. Sjöström, G. G. Turrigiano, S. B. Nelson, Rate, timing, and cooperativity jointly determine cortical synaptic plasticity. *Neuron* **32**, 1149–1164 (2001).

11. D. O. Hebb, *The Organization of Behavior: A Neuropsychological Theory* (Psychology Press, 2005).

12. Y. Dan, M.-M. Poo, Spike timing-dependent plasticity of neural circuits. *Neuron* **44**, 23–30 (2004).

13. G. Koch, V. Ponzo, F. Di Lorenzo, C. Caltagirone, D. Veniero, Hebbian and anti-Hebbian spike-timing-dependent plasticity of human cortico-cortical connections. *J. Neurosci.* **33**, 9725–9733 (2013).

14. P. D. Roberts, T. K. Leen, Anti-hebbian spike-timing-dependent plasticity and adaptive sensory processing. *Front. Comput. Neurosci.* **4**, 156 (2010).

15. M. Graupner, N. Brunel, Calcium-based plasticity model explains sensitivity of synaptic changes to spike pattern, rate, and dendritic location. *Proc. Natl. Acad. Sci. U. S. A.* **109**, 3991–3996 (2012).

16. Watson BO, Levenstein D, Greene JP, Gelinas JN, Buzsáki G. (2016); Multi-unit spiking activity recorded from rat frontal cortex (brain regions mPFC, OFC, ACC, and M2) during wake-sleep episode wherein at least 7 minutes of wake are followed by 20 minutes of sleep. CRCNS.org.http://dx.doi.org/10.6080/K02N506Q.

17. F. Tatsuki, G. A. Sunagawa, S. Shi, E. A. Susaki, H. Yukinaga, D. Perrin, K. Sumiyama, M. Ukai-Tadenuma, H. Fujishima, R.-I. Ohno, D. Tone, K. L. Ode, K. Matsumoto, H. R. Ueda, Involvement of Ca(2+)-Dependent Hyperpolarization in Sleep Duration in Mammals. *Neuron* **90**, 70–85 (2016).

18. L. B. Krone, T. Yamagata, C. Blanco-Duque, M. C. C. Guillaumin, M. C. Kahn, V. van der Vinne, L. E. McKillop, S. K. E. Tam, S. N. Peirson, C. J. Akerman, A. Hoerder-Suabedissen, Z. Molnár, V. V. Vyazovskiy, A role for the cortex in sleep-wake regulation. *Nat. Neurosci.* **24**, 1210–1215 (2021).

19. G. H. Diering, R. S. Nirujogi, R. H. Roth, P. F. Worley, A. Pandey, R. L. Huganir, Homer1a drives homeostatic scaling-down of excitatory synapses during sleep. *Science* **355**, 511–515 (2017).

20. F. Brüning, S. B. Noya, T. Bange, S. Koutsouli, J. D. Rudolph, S. K. Tyagarajan, J. Cox, M. Mann, S. A. Brown, M. S. Robles, Sleep-wake cycles drive daily dynamics of synaptic phosphorylation. *Science* **366** (2019).

21. A. A. Borbély, A two process model of sleep regulation. *Hum. Neurobiol.* **1**, 195–204 (1982).

22. K. L. Ode, H. R. Ueda, Phosphorylation Hypothesis of Sleep. *Front. Psychol.* **11**, 575328 (2020).

23. D. Tone, K. L. Ode, Q. Zhang, H. Fujishima, R. G. Yamada, Y. Nagashima, K. Matsumoto, Z. Wen, S. Y. Yoshida, T. T. Mitani, Y. Arisato, R.-I. Ohno, M. Ukai-Tadenuma, J. Yoshida Garçon, M. Kaneko, S. Shi, H. Ukai, K. Miyamichi, T. Okada, K. Sumiyama, H. Kiyonari, H. R. Ueda, Distinct phosphorylation states of mammalian CaMKIIβ control the induction and maintenance of sleep. *PLoS Biol.* **20**, e3001813 (2022).

24. A. Hudmon, H. Schulman, Neuronal CA2+/calmodulin-dependent protein kinase II: the role of structure and autoregulation in cellular function. *Annu. Rev. Biochem.* **71**, 473–510 (2002).

25. C. Cirelli, C. M. Gutierrez, G. Tononi, Extensive and divergent effects of sleep and wakefulness on brain gene expression. *Neuron* **41**, 35–43 (2004).

26. K. B. Hengen, M. E. Lambo, S. D. Van Hooser, D. B. Katz, G. G. Turrigiano, Firing rate homeostasis in visual cortex of freely behaving rodents. *Neuron* **80**, 335–342 (2013).

27. V. V. Vyazovskiy, U. Olcese, Y. M. Lazimy, U. Faraguna, S. K. Esser, J. C. Williams, C. Cirelli, G. Tononi, Cortical firing and sleep homeostasis. *Neuron* **63**, 865–878 (2009).

28. V. V. Vyazovskiy, C. Cirelli, M. Pfister-Genskow, U. Faraguna, G. Tononi, Molecular and electrophysiological evidence for net synaptic potentiation in wake and depression in sleep.

Nat. Neurosci. **11**, 200–208 (2008).

29. L. de Vivo, M. Bellesi, W. Marshall, E. A. Bushong, M. H. Ellisman, G. Tononi, C. Cirelli, Ultrastructural evidence for synaptic scaling across the wake/sleep cycle. *Science* **355**, 507–510 (2017).

30. S. J. Aton, J. Seibt, M. Dumoulin, S. K. Jha, N. Steinmetz, T. Coleman, N. Naidoo, M. G. Frank, Mechanisms of sleep-dependent consolidation of cortical plasticity. *Neuron* **61**, 454–466 (2009).

31. M. Massimini, F. Amzica, Extracellular calcium fluctuations and intracellular potentials in the cortex during the slow sleep oscillation. *J. Neurophysiol.* **85**, 1346–1350 (2001).

32. R. Havekes, S. J. Aton, Impacts of Sleep Loss versus Waking Experience on Brain Plasticity: Parallel or Orthogonal? *Trends Neurosci.* **43**, 385–393 (2020).

33. A. Suppermpool, D. G. Lyons, E. Broom, J. Rihel, Sleep pressure modulates single-neuron synapse number in zebrafish. *Nature* **629**, 639–645 (2024).

34. R. M. Mulkey, S. Endo, S. Shenolikar, R. C. Malenka, Involvement of a calcineurin/inhibitor-1 phosphatase cascade in hippocampal long-term depression. *Nature* **369**, 486–488 (1994).

35. J. Tomita, M. Mitsuyoshi, T. Ueno, Y. Aso, H. Tanimoto, Y. Nakai, T. Aigaki, S. Kume, K. Kume, Pan-Neuronal Knockdown of Calcineurin Reduces Sleep in the Fruit Fly, Drosophila melanogaster. *J. Neurosci.* **31**, 13137–13146 (2011).

36. Y. Wang, S. Cao, D. Tone, H. Fujishima, R. G. Yamada, R.-I. Ohno, S. Shi, K. Matsuzawa, M. Kaneko, M. Ukai-Tadenuma, H. Ukai, C. Hanashima, H. Kiyonari, K. Sumiyama, K. L. Ode, H. R. Ueda, Post-synaptic competition between calcineurin and PKA regulates mammalian sleep-wake cycles, *bioRxiv* (2023)p. 2023.12.21.572751.

37. A. M. Strijkstra, S. Daan, Dissimilarity of slow-wave activity enhancement by torpor and sleep deprivation in a hibernator. *Am. J. Physiol.* **275**, R1110-7 (1998).

38. C. G. von der Ohe, C. Darian-Smith, C. C. Garner, H. C. Heller, Ubiquitous and temperature-dependent neural plasticity in hibernators. *J. Neurosci.* **26**, 10590–10598 (2006).

39. J.-G. He, H.-Y. Zhou, F. Wang, J.-G. Chen, Dysfunction of glutamatergic synaptic transmission in depression: Focus on AMPA receptor trafficking. *Biol. Psychiatry Glob. Open Sci.* **3**, 187–196 (2023).

40. T. Tadros, M. Bazhenov, Role of Sleep in Formation of Relational Associative Memory. *J. Neurosci.* **42**, 5330–5345 (2022).

41. J. F. A. Poulet, C. C. H. Petersen, Internal brain state regulates membrane potential synchrony in barrel cortex of behaving mice. *Nature* **454**, 881–885 (2008).

42. L. Aitchison, J. Jegminat, J. A. Menendez, J.-P. Pfister, A. Pouget, P. E. Latham, Synaptic plasticity as Bayesian inference. *Nat. Neurosci.* **24**, 565–571 (2021).

43. D. Festa, A. Aschner, A. Davila, A. Kohn, R. Coen-Cagli, Neuronal variability reflects probabilistic inference tuned to natural image statistics. *Nat. Commun.* **12**, 3635 (2021).

44. B. L. Sabatini, T. G. Oertner, K. Svoboda, The life cycle of Ca(2+) ions in dendritic spines. *Neuron* **33**, 439–452 (2002).

45. D. Levenstein, G. Buzsáki, J. Rinzel, NREM sleep in the rodent neocortex and hippocampus reflects excitable dynamics. *Nat. Commun.* **10**, 2478 (2019).

46. V. Crunelli, M. L. Lörincz, A. C. Errington, S. W. Hughes, Activity of cortical and thalamic neurons during the slow (<1 Hz) rhythm in the mouse in vivo. *Pflugers Arch.* **463**, 73–88 (2012).

47. F. Helmchen, K. Imoto, B. Sakmann, Ca2+ buffering and action potential-evoked Ca2+ signaling in dendrites of pyramidal neurons. *Biophys. J.* **70**, 1069–1081 (1996).

48. S. Song, P. J. Sjöström, M. Reigl, S. Nelson, D. B. Chklovskii, Highly nonrandom features of synaptic connectivity in local cortical circuits. *PLoS Biol.* **3**, e68 (2005).

49. H. W. Kessels, R. Malinow, Synaptic AMPA receptor plasticity and behavior. *Neuron* **61**, 340–350 (2009).

50. P. Franken, D. Chollet, M. Tafti, The homeostatic regulation of sleep need is under genetic control. *J. Neurosci.* **21**, 2610–2621 (2001).

Acknowledgments

We thank all the laboratory members at RIKEN Center for Biosystems Dynamics Research and the University of Tokyo. We thank M. Graupner for guidance of codes. We thank B. O. Watson and D. Levenstein for guidance of in vivo datasets. We thank MN Ballester Roig for reviewing manuscripts. We thank G. Buzsáki, V. V. Vyazovskiy, C. Cirelli, G. H. Diering, P. Meerlo, P. Franken, M. G. Frank, A. Adamantidis, H. C. Heller, M. Schmidt and A. Loudon for helpful discussions.

Funding:

JST ERATO grant number JPMJER2001

the Science and Technology Platform Program for Advanced Biological Medicine (AMED/MEXT to H.R.U.)

a Grant-in-aid for scientific research (S) (to H.R.U., grant number JP18H05270)

MEXT Quantum Leap Flagship Program (MEXT QLEAP) (to H.R.U., grant number JPMXS0120330644)

a Grant-in-Aid from the Human Frontier Science Program (to H.R.U.)

RIKEN Junior Research Associate Program.

Author Contributions:

Conceptualization: F.L.K., R.G.Y., and H.R.U.

Methodology: F.L.K., R.G.Y., K.L.O., and H.R.U.

Simulation: F.L.K.; Validation: F.L.K., R.G.Y., and K.L.O.

Writing (original draft): F.L.K.

Writing (review and editing): F.L.K., R.G.Y., K.L.O., and H.R.U

Competing interests: The authors declare that they have no competing interests.

Supplementary Materials

Materials and Methods

Supplementary Text

Figs. S1 to S20

Tables S1 to S8

References

Figures

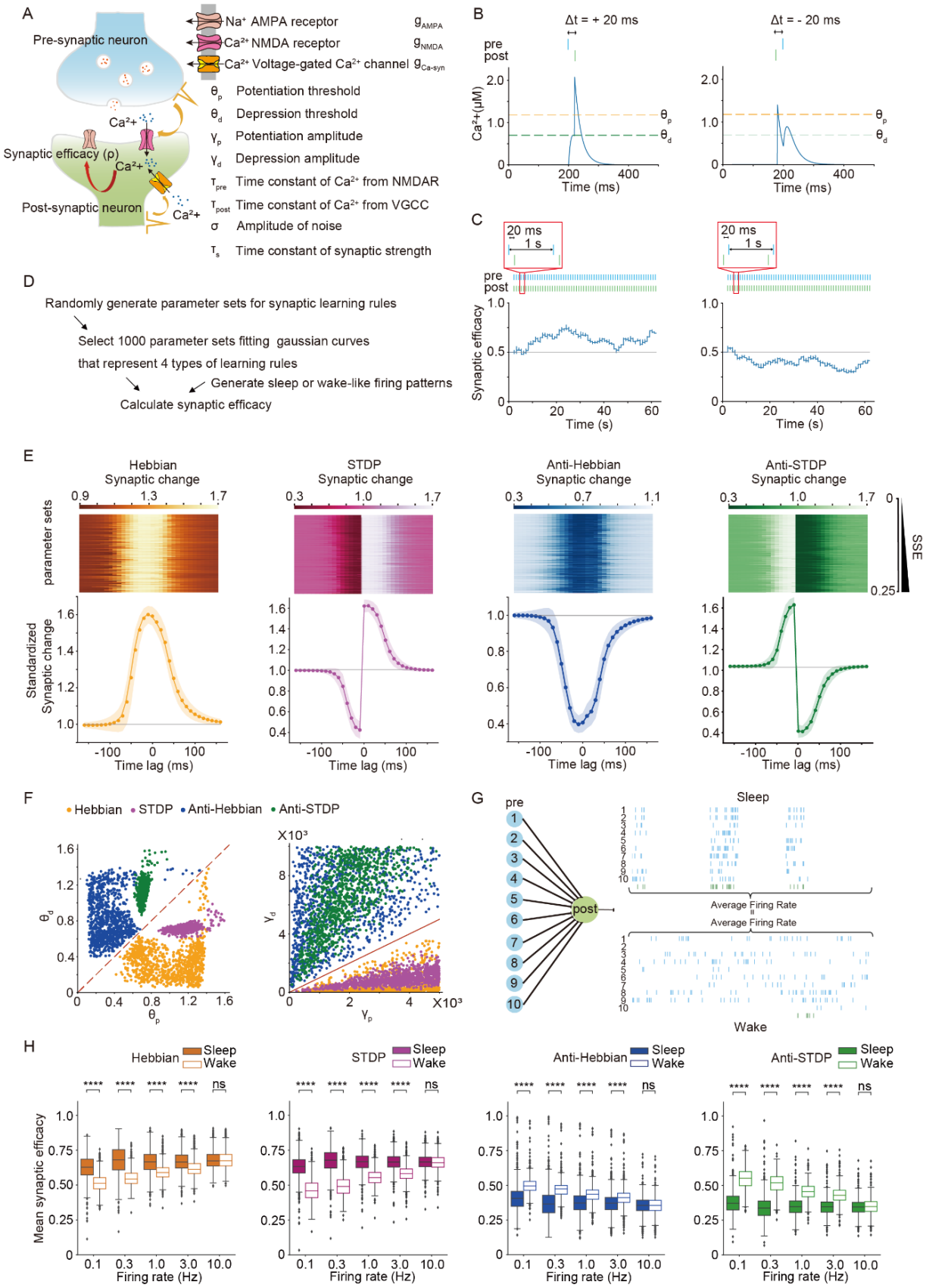
A
Pre-synaptic neuron
Ca²+
Synaptic efficacy (ρ)
Post-synaptic neuron
Na+ AMPA receptor
Ca²+ NMDA receptor
Ca²+ Voltage-gated Ca²+ channel
Potentiation threshold
Depression threshold
Potentiation amplitude
Depression amplitude
Time constant of Ca²+ from NMDAR
Time constant of Ca²+ from VGCC
Amplitude of noise
Time constant of synaptic strength
B
Δt = + 20 ms
Δt = - 20 ms
pre
post
Ca²+(μM)
Time (ms)
C
20 ms
1 s
Synaptic efficacy
Time (s)
D
Randomly generate parameter sets for synaptic learning rules
Select 1000 parameter sets fitting gaussian curves
that represent 4 types of learning rules
Generate sleep or wake-like firing patterns
Calculate synaptic efficacy
E
Hebbian
STDP
Anti-Hebbian
Anti-STDP
Synaptic change
parameter sets
SSE
Standardized Synaptic change
Time lag (ms)
F
Hebbian
STDP
Anti-Hebbian
Anti-STDP
X10³
G
pre
post
Sleep
Average Firing Rate
Wake
H
Hebbian
STDP
Anti-Hebbian
Anti-STDP
Sleep
Wake
Mean synaptic efficacy
Firing rate (Hz)
****
ns

Fig. 1. WISE under Hebbian and STDP, SHY under Anti-Hebbian and Anti-STDP assuming the same firing rates during sleep-like and wake-like firing patterns.

(**A**) Schematic illustration of the Ca^{2+}-based plasticity model for synaptic learning rules.

(B) Calcium transients in a post-neuronal synapse when stimulated with short delays under STDP.

(C) The dynamics of synaptic efficacy when stimulated with short delays under STDP.

(D) The procedure of a parameter search for synaptic learning rules and calculation of synaptic efficacy in the state of sleep and wake.

(E) The standardized synaptic change of the 1000 parameter sets for four types of learning rules represented by Gaussian curves. Each row of the upper panels shows synaptic changes simulated with a parameter set whose sum of squared errors (SSE) between analytical results and Gaussian curves was less than 0.25. The line and shadow in the lower panel indicate the mean and standard deviation, respectively.

(F) Distributions of 1000 parameter sets for each learning rule in the axes of thresholds and amplitudes.

(G) Schematic illustration for connections and firing patterns of neurons used in the calculation of synaptic efficacy.

(H) Box plots for mean synaptic efficacy in sleep-like and wake-like firing patterns by different synaptic learning rules and mean firing rates (n=1000 for each firing rate). The whiskers above and below show minimal to maximal values. The box extends from the 25th to the 75th percentile, and the middle line indicates the median. * $p < 0.05$, ** $p < 0.01$, *** $p < 0.001$, **** $p < 0.0001$, Welch's t-test was applied.

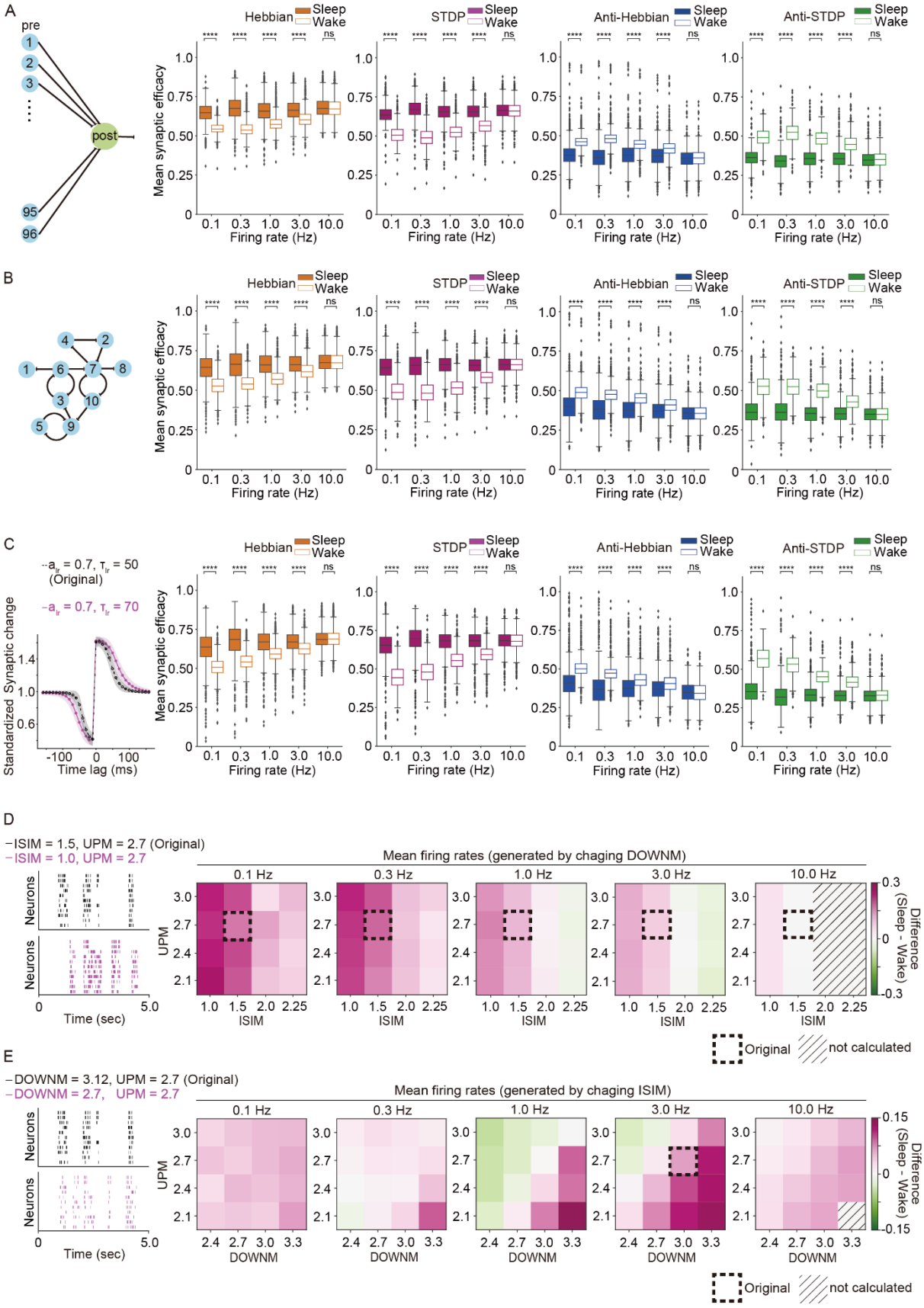
A
pre
post
Hebbian
STDP
Anti-Hebbian
Anti-STDP
Sleep
Wake
Mean synaptic efficacy
Firing rate (Hz)
B
C
Standardized Synaptic change
Time lag (ms)
D
Mean firing rates (generated by chaging DOWNM)
UPM
ISIM
Neurons
Time (sec)
Difference (Sleep - Wake)
Original
not calculated
E
Mean firing rates (generated by chaging ISIM)
DOWNM

Fig. 2. Robustness of WISE and SHY.

(**A**) Schematic illustration of network model consisting of one post-neuron connected with 96 pre-neuronal synapses and box plots for synaptic efficacy.

(B) Schematic illustration of neural network model consisting of randomly connected ten neurons and box plots for synaptic efficacy.

(C) The original (black dotted line) and modified (magenta solid line) curves for STDP rule and box plots for mean synaptic efficacy. a_{lr} is the amplitude, and τ_{lr} is the time constant for Gaussian curves to be fitted by the parameter search.

(D) Representative raster plots of the original (black) and modified (magenta) sleep-like firing patterns and the differences in median of mean synaptic efficacies between sleep-like and wake-like firing patterns (*sleep - wake*). The modified mean firing rates of sleep-like firing patterns were generated by changing DOWNM under constant UPM and ISIM (n=1000 for each firing rate). The dotted boxes highlighted the original UPM and ISIM values are 1.5 and 2.7, respectively.

(E) Representative raster plots of the original (black) and modified (magenta) sleep-like firing patterns and the differences in median of mean synaptic efficacies between sleep-like and wake-like firing patterns (*sleep - wake*). The modified firing rates of sleep-like patterns were generated by changing ISIM under constant UPM and DOWNM (*n=1000* for each firing rate). The dotted boxes highlighted *DOWNM =3.0* and *UPM = 2.7*, which are the closest to the original values: *DOWNM = 3.12* and *UPM = 2.7*.

(A to C) The mean synaptic efficacy was evaluated in sleep-like and wake-like firing patterns with various mean firing rates assuming different synaptic learning rules (*n=1000* for each firing rate). The whiskers above and below of box plots show minimal and maximal values, respectively. The box extends from the 25th to the 75th percentile and the middle line indicates the median. * $p < 0.05$, ** $p < 0.01$, *** $p < 0.001$, **** $p < 0.0001$, Welch's t-test was applied.

(D and E) ISIM: log10(*mean ISI*), UPM: log10(*mean Up-state duration*), DOWNM: log10(*mean Down-state duration*)

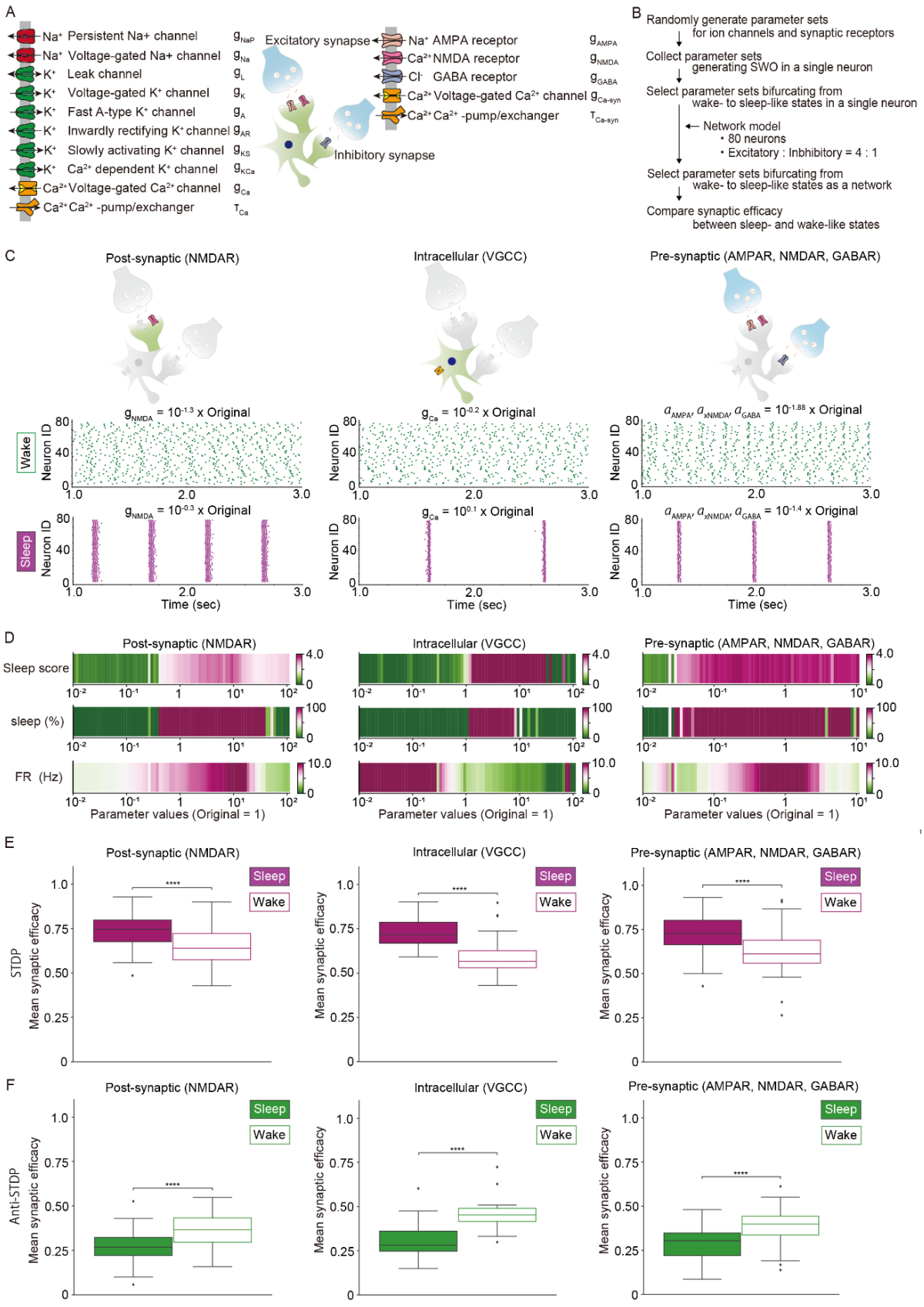
A
Na+ Persistent Na+ channel
Na+ Voltage-gated Na+ channel
K+ Leak channel
K+ Voltage-gated K+ channel
K+ Fast A-type K+ channel
K+ Inwardly rectifying K+ channel
K+ Slowly activating K+ channel
K+ Ca2+ dependent K+ channel
Ca2+ Voltage-gated Ca2+ channel
Ca2+ Ca2+ -pump/exchanger
Excitatory synapse
Na+ AMPA receptor
Ca2+ NMDA receptor
Cl- GABA receptor
Ca2+ Voltage-gated Ca2+ channel
Ca2+ Ca2+ -pump/exchanger
Inhibitory synapse
B
Randomly generate parameter sets for ion channels and synaptic receptors
Collect parameter sets generating SWO in a single neuron
Select parameter sets bifurcating from wake- to sleep-like states in a single neuron
Network model
• 80 neurons
• Excitatory : Inbhibitory = 4 : 1
Select parameter sets bifurcating from wake- to sleep-like states as a network
Compare synaptic efficacy between sleep- and wake-like states
C
Post-synaptic (NMDAR)
Intracellular (VGCC)
Pre-synaptic (AMPAR, NMDAR, GABAR)
Wake
Sleep
Neuron ID
Time (sec)
D
Sleep score
sleep (%)
FR (Hz)
Parameter values (Original = 1)
E
STDP
Mean synaptic efficacy
Sleep
Wake
F
Anti-STDP
Mean synaptic efficacy

527

Fig. 3. WISE and SHY in Hodgkin-Huxley-based network models.

(**A**) Schematic illustration of a model with excitatory and inhibitory synapses. A Hodgkin-Huxley-based network model was constructed based on the averaged neuron model in a previous study (*17*).

(B) Procedures for collecting parameter sets that bifurcate from wake-like to sleep-like firing patterns and comparing synaptic efficacy between the two states in Hodgkin-Huxley-based network models.

(C) Representative sleep-like and wake-like firing patterns for three types of bifurcation models. The parameters used in the simulation were obtained by multiplying the original values defined in Table S5 by the presented factors. Simulations were conducted for five seconds and presented for three seconds in each model.

(D) Changes in the sleep score, percentage of sleep-like waveforms (sleep (%)), and mean firing rate (FR (Hz)) as the conductance of the channel or receptor, or the coefficients of pre-synaptic activations are gradually increased. The range of the conductance was divided into 80 steps for post-synaptic or intracellular bifurcation, while the range of the coefficient was divided into 75 steps for pre-synaptic bifurcation. Simulations were conducted for ten seconds at each conductance or coefficient step.

(E and F) Box plots for mean synaptic efficacy during sleep-like and wake-like firing patterns under STDP (E) and Anti-STDP (F) by three types of network models (n = 191, 52, and 150 for STDP and n = 121, 36, and 119 for Anti-STDP in post-synaptic, intracellular, and pre-synaptic bifurcation models, respectively). The whiskers above and below of box plots show minimal and maximal values, respectively. The box extends from the 25th to the 75th percentile, and the middle line indicates the median. * $p < 0.05$, ** $p < 0.01$, *** $p < 0.001$, **** $p < 0.0001$, Student's t-test was applied.

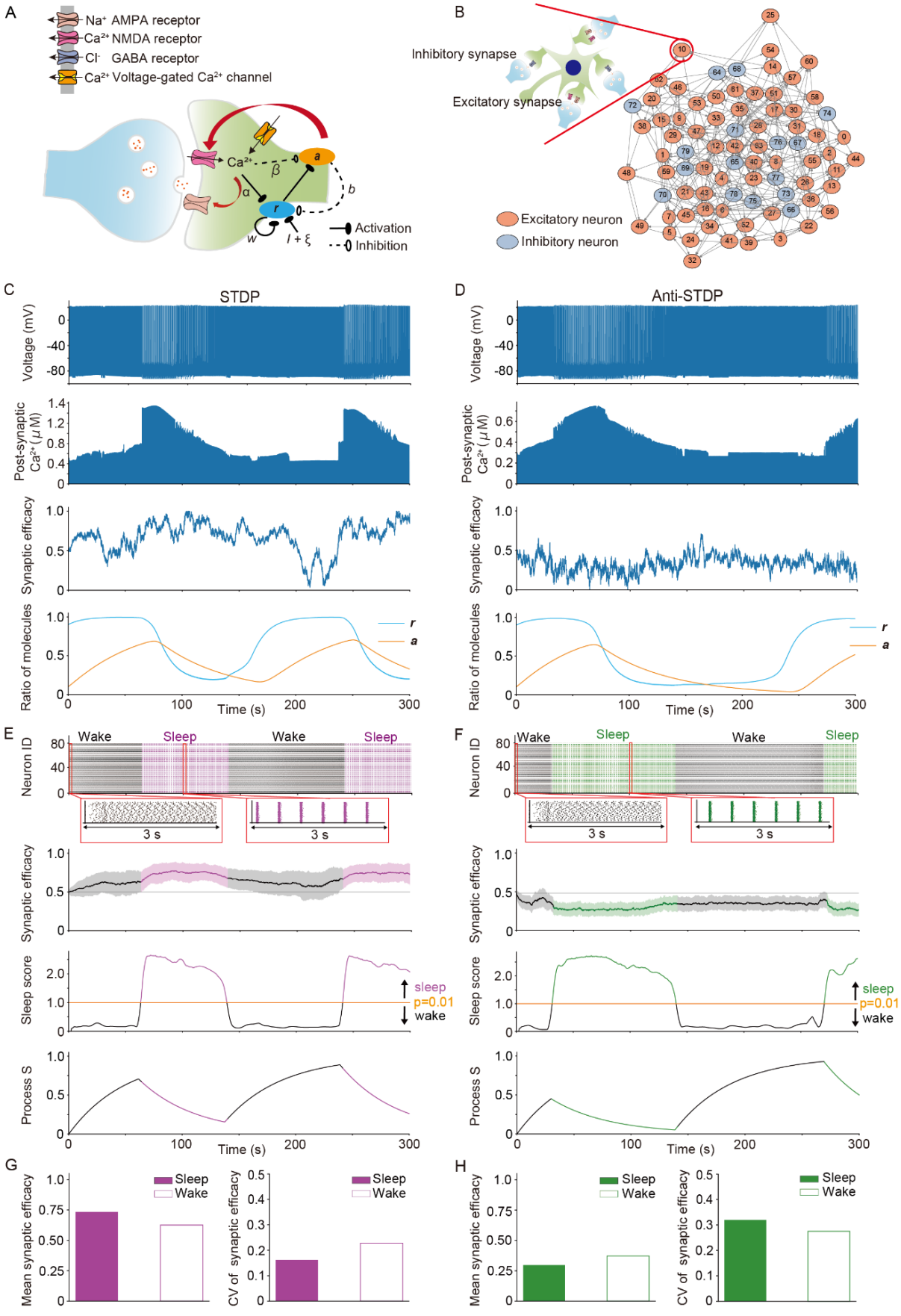
A
Na+ AMPA receptor
Ca2+ NMDA receptor
Cl- GABA receptor
Ca2+ Voltage-gated Ca2+ channel
Activation
Inhibition
B
Inhibitory synapse
Excitatory synapse
Excitatory neuron
Inhibitory neuron
C
STDP
D
Anti-STDP
Voltage (mV)
Post-synaptic Ca2+ (μM)
Synaptic efficacy
Ratio of molecules
Time (s)
E
F
Neuron ID
Wake
Sleep
3 s
Sleep score
sleep
p=0.01
wake
Process S
G
H
Mean synaptic efficacy
CV of synaptic efficacy

552

Fig. 4. WISE under Hebbian and STDP and SHY under Anti-Hebbian and Anti-STDP is compatible with models including sleep-wake dynamics.

(**A**) Schematic illustration of the model for sleep-wake dynamics in excitatory synapses. The initial state of CaMKII such as pT286/287 CaMKII is represented by ***r.*** The initial state activates ***a*** which corresponds to the second state of CaMKII such as pT305/306 CaMKII or phosphatases such as calcineurin. α, β, *w*, and *b* corresponds to variables defined in the equations in the supplementary text III. Synaptic efficacies were calculated in Hodgkin-Huxley-based network models bifurcated by the post-synaptic mechanism with sleep-wake dynamics under synaptic learning rules. The conductance of NMDAR was updated by ***a*** and the simulations were optimized by Pearson's correlation coefficients between process S and ***r***. The simulations were conducted for 500 seconds. The parameter set for channel or receptor conduces, learning rule and sleep-wake dynamics and initial values for variables in a representative model are shown in table S5 to S8.

(B) Schematic illustration of the network model used in simulations. The network model has 80 neurons with the E:1 ratio of 4:1.

(C and D) Time changes of post-synaptic membrane potential and Ca^{2+} concentration, synaptic efficacy, and the ratio of two phosphorylated states of kinases (***r*** and ***a***) of a synapse in representative network models under STDP (C) and Anti-STDP (D). The results of 0-300 seconds are shown.

(E and F) Raster plots and time changes of mean synaptic efficacy, sleep score, and process S in representative network models under STDP (E) and Anti-STDP (F). The shadow in time changes in mean synaptic efficacy represents SD. The network was considered to be in the state of sleep or wake if the sleep score was above or below the threshold, respectively (the threshold is the value of sleep score where p = 0.01; see supplementary text IV). The results of 0-300 seconds are shown.

(G and H) Mean and coefficient of variance (CV) of synaptic efficacy during the periods of sleep-like and wake-like states in representative network models under STDP (E) and Anti-STDP (F).

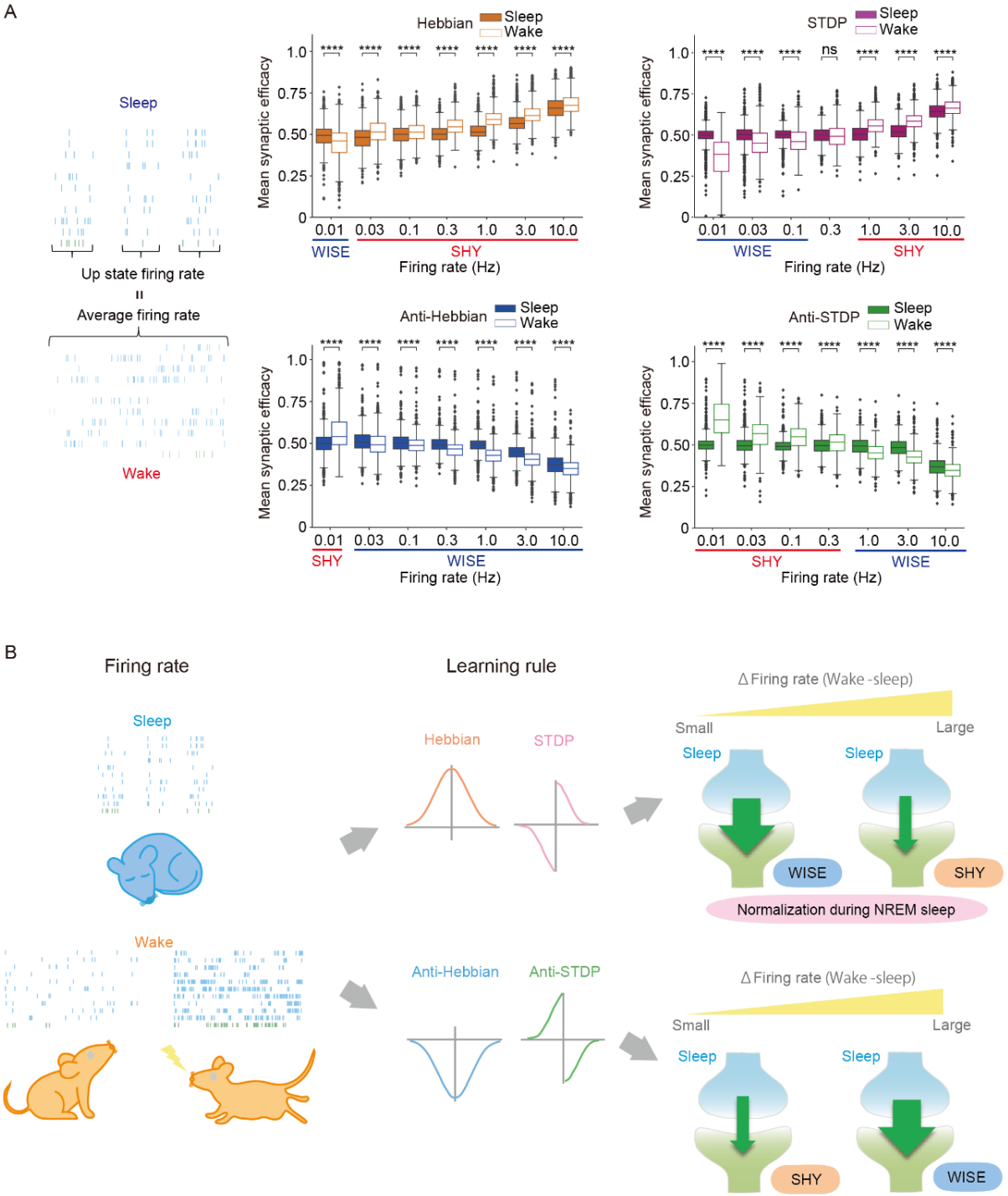

596

597 **Fig. 5. Synaptic changes depend on firing rates assuming higher firing rates during**
598 **wakefulness.**

599 (**A**) A Schematic illustration for sleep-like and wake-like spike patterns and box plots for mean
600 synaptic efficacy in sleep-like and wake-like firing patterns for different learning rules and mean
601 firing rates (n=1000 for each firing rate). The mean firing rates in wake-like states are equal to the

mean firing rates in Up states of sleep-like states. The sleep-like firing patterns were generated by sampling from the lognormal distributions with log10(*mean Up-state duration*) = 2.7 and log10(*mean Down-state duration*) = 3.0. SD was calculated according to the linear regression analysis based on in vivo data (fig. S18).

WISE and SHY dynamics are highlighted under the x-axis according to the change in the direction of synaptic efficacy. The whiskers above and below show minimal to maximal values. The box extends from the 25th to the 75th percentile and the middle line indicates the median. * $p < 0.05$, ** $p < 0.01$, *** $p < 0.001$, **** $p < 0.0001$, Welch's t-test was applied.

(B) A Graphical abstract of a unified framework for synaptic dynamics during the sleep-wake cycle. SHY: Synaptic homeostasis hypothesis, WISE: Wake Inhibition Sleep Excitation